Excited state localisation cascades in inorganic semiconductor nanoparticles

Martijn A. Zwijnenburg

Department of Chemistry and Thomas Young Centre, University College London, 20 Gordon Street, WC1H 0AJ, UK. Email address: m.zwijnenburg@ucl.ac.uk.

Abstract

Excited state relaxation in zinc sulfide (ZnS) nanoparticles is studied as a model for the fate of excited state in inorganic nanoparticles in general. A series of time-dependent density functional theory optimisations on the S_1 and T_1 excited states predict the existence of not merely isolated minima, as found before, but rather a connected cascade of excited state minima ending up in a conical intersection between the excited state energy surface and the ground state. The localisation of the excited state in the different minima increases down the cascade, while the barriers separating these minima, studied here for the first time, are predicted to be in some cases electronic (strongly avoided crossing) in origin. The cartoon picture of excited state relaxation in inorganic nanoparticles that involves relaxation to the bottom of only one approximately harmonic well followed by photoluminescence appears for the ZnS nanoparticles studied here to be a best rather simplistic. The localisation cascade is finally found to strongly affect the excited state properties of nanoparticles and predicted to lead to the formation of defected nanoparticles after de-excitation in selected cases.

Introduction

Applications of nanoparticles in photocatalysis[1,2,3], photovoltaics[4,5,6] and as photoluminescent markers[7,8,9] all involve the generation and subsequent exploitation of excited electron and hole pairs. In photocatalysis excited electrons are, for example, used to reduce protons to molecular hydrogen and the holes to oxidise water to molecular oxygen. To properly understand the physical and chemical processes underlying these applications and the influence of material properties (e.g. nanoparticle size, shape composition) on the obtained results, it is crucial to properly comprehend the fate of the excited nanoparticles after excitation.

After excitation a number of processes will occur (see Fig. 1) (*i*) radiationless relaxation from higher excited states to the lowest excited state (e.g. from S_n to S_1, where the S signifies singlet states) if the nanoparticle was initially excited into a higher excited state than the lowest excited state, (*ii*) relaxation on the S_1 excited state energy surface to a nearby S_1 minima or S_1/S_0 conical intersection (CX and (*iii*) either radiative relaxation back to S_0 in the case of the minimum (photoluminescence, PL, fluorescence) or raditionless relaxation back to S_0 in the case of the CX. Moreover, there is also the potential for (*iv*) an intersystem crossing from the S_1 to T_1 surface, followed (*v*) by relaxation on the T_1 excited state energy surface to a nearby minimum and (*vi*) radiative relaxation to S_0 (PL, phosphorescence). Furthermore, in the case of (*iii*) and (*vi*) there is a chance that after relaxation back to S_0 there is no barrier-less downhill path back to the original S_0 structure and the nanoparticle ends up in a different S_0 minimum and thus with a modified ground state structure. The relaxation from S_n to S_1 through internal conversion (IC, process (*i*)) is generally very fast so that we can treat processes (*i*) and (*ii*) as happening subsequently. This observation is canonised in Kasha's rule[10], which states that fluorescence or phosphorescence occurs in appreciable yield only from the lowest excited state of a given multiplicity (i.e. S_1 or T_1). The vast majority of

systems appear to follow Kasha's rule though selected experimental examples of non–Kasha behaviour are known for molecules[11] and more recently also nanoparticles[12]. In the remainder of the paper we will assume Kasha's rule to hold and exclusively focus on the S_1 and T_1 excited state energy landscapes.

Taking into account the amount of papers showcasing excited state applications of nanoparticles, we know surprisingly little about the underlying atomistic and electronic processes outlined above. From an experimental perspective the problem is twofold. Firstly, most scattering and spectroscopic methods yield only an average picture of the atomic structure while nanostructures are often severely disordered and, due to their small size, show limited long-range order. Secondly, excited state processes are inherently transient in nature. Structures relevant to the excited state processes (e.g. those for (*iii*), (*iv*) and (*vi*)) often only exist for very short times which makes them especially difficult to characterise. Computational calculations do not suffer from these problems. One can employ global optimisation algorithms to predict nanoparticle structures without recourse to experiment. The development of time-dependent density functional theory[13] (TD-DFT) in general and the derivation of analytical expressions for the nuclear gradients in particular[14,15,16] (and the incorporation of code for calculating such gradients in standard quantum chemistry codes) has made an exploration of the excited state landscape of true nanoparticles (i.e. larger than 1 nm) numerically tractable. Such calculations provide an opportunity to revolutionise understanding, as has occurred for applications that do not involve excited states (e.g. conventional heterogeneous catalysis). Recent years have, therefore, seen a number of publications[17-24] studying the excited-state energy landscape of nanoparticles in the so-called Franck-Condon region, i.e. in the direct neighbourhood of the ground state minimum.

Here I report on the first explicit exploration of the excited state energy landscape of inorganic nanoparticles beyond this Franck-Condon region and show that in practice for our

model system of choice (~1-2 nm Zinc Sulfide, ZnS, particles, which experimentally are known to display PL at 420–520 nm, i.e. 3.0–2.4 eV,[25-31] and to be active as photocatalysts[32,33]) there is a cascade of minima including, for the first time, what appears to be a CX, where the S_1 and S_0 energy surfaces cross. There is no inherent reason why a similar cascade of excited state minima, where the excited state becomes trapped on increasingly smaller number of atoms, could not occur for larger nanoparticles or inorganic nanoparticles of other materials than ZnS. Furthermore, the relative height of the excited state barriers between the different excited state minima is obtained, to my knowledge a first for nanoparticles. These barriers height values allow one to not only consider energetics but also for the first time to make informed statements about excited state kinetics. Finally, an example is presented where relaxation on the ground state energy surface after de-excitation is predicted to lead to an alternate ground state minimum and discuss the general impact of a localisation cascade on the physical and chemical properties of inorganic nanoparticles.

Previous computational work on ZnS nanoparticles

This work builds further on a series of previous computational publications that have focussed upon ZnS nanoparticles as model systems for inorganic semiconductor nanoparticles in general[22,23,24,34] (which in itself form part of a much larger body of papers focussing mostly on vertical excitation spectra of selected ZnS nanostructures[35-40]). In these publications it was shown that TD-DFT predicts the experimentally measured optical absorption spectra of small ZnS nanoparticles and that TD-DFT predictions are consistent with those obtained using correlated wavefunction methods (complete active space self-consistent field second-order perturbation theory and approximate coupled cluster methods) for sub-nanometre clusters. They also include a study of the Franck-Condon region of both naked ($Zn_{12}S_{12}$, $Zn_{16}S_{16}$, $Zn_{22}S_{22}$ and $Zn_{26}S_{26}$) and hydrated ($(Zn_{12}S_{12})(H_2O)_{12}$ and $(Zn_{16}S_{16})(H_2O)_{16}$) ZnS global minima candidates (previously enumerated in references 24, 34

and 41-46), which showed that larger (r > 1 nm) and hydrated particles reproduce the experimentally observed PL[24]. Furthermore, two fundamentally different S_1 excited state minima have been reported for these nanoparticles, both involving a 4-membered ring[24]. The smaller nanoparticles display one type of minimum, which involve an electron predominantly localised on one zinc atom of a 4-membered ring and the hole evenly localised on two adjacent sulfur atoms (we refer to this as a *I-II* type minimum, where the Roman numerals indicate upon how many atoms the electron and hole respectively predominantly are trapped, see also section ESI-1 of the supplementary information). For the larger clusters, two minima were found. One at higher energy, where the hole gets evenly trapped on two sulfur atoms of a 4-membered ring while the electron remains delocalised, though not evenly, over all zinc atoms (a *N-II* minimum, where *N* stands for "nulla", Latin for none), and a lower energy *I-II* type minimum. For T_1, in contrast, for all particles only a *I-II* type minimum was observed. In this study we additionally find type *I-I* minima for T_1 and type *I-I* CXs for S_1, both never before observed for ZnS or other inorganic nanoparticles, and new versions of the type *N-II* and *I-II* minima. More importantly, we explore the interrelatedness between minima, estimate the barriers that separate them and generally make a first exploration of the complexity of the excited state energy landscape of ZnS nanoparticles.

Computational details

We explored the minima and barriers on the excited state energy landscape of four specific ~ 1 - 2 nm ZnS nanoparticles; the likely global minima isomers of the bare $Zn_{12}S_{12}$, $Zn_{16}S_{16}$, $Zn_{22}S_{22}$ and $Zn_{26}S_{26}$ particles (see Fig. 2), also studied in previous work[24,34]. All the DFT/TD-DFT calculations were performed using the Turbomole[47-50] 6.3.1 code, and, employed the hybrid B3LYP[51] exchange-correlation (XC-)functional and the DZ(D)P[52] basis-set. For triplet states we employed the Tamn-Dancoff approximation to TD-DFT, as this is known from the literature to give more stable results for triplet states than full TD-DFT[53,54]. Relaxations, both

those of the ground and excited states, were continued until the maximum norm of the Cartesian gradients was smaller than $1x10^{-5}$ Hartree/Bohr ($1x10^{-4}$ Hartree/Bohr for $Zn_{22}S_{22}$ and $Zn_{26}S_{26}$). Finally, where numerically tractable, (numerical) frequency calculations were performed to verify that stationary points obtained by relaxation of the ground and excited state correspond to proper minima.

Information on the degree of localisation in the excited state were obtained by means of the difference in between the Natural Population Analysis charges of a nanoparticle in the ground and excited state for the same geometry. Estimates of the energetic barriers between different minima on the S_1 excited state energy surface were obtained in a two-step procedure. First, interpolation using the interpolate function of the molecular structure manipulation toolkit[55] was used to obtain an upper limit to the barrier height and initial guess for step two. Typically ten structures are used in the interpolation and care is taken that the excited state is localised on the same sub-set of atoms in both minima. In the second step a numerical frequency calculation was performed followed by a Trust-Region Image Minimization[56] (TRIM) transition state search along the (lowest) imaginary frequency found in the frequency calculation. Afterwards, a final frequency calculation was performed to confirm that the obtained transition state structure has only one imaginary frequency. Finally, for selected cases we slightly distorted the obtained transition state structures in both directions along the imaginary mode (using the Turbomole screwer tool), started excited state optimisation runs from these distorted structures and verified that these runs end up in the two minima that the transition state is meant to connect.

Canonical Born-Oppenheimer molecular dynamics (BOMD) for S_1 state of the $Zn_{12}S_{12}$ nanoparticle were obtained at 10 K using the Frog module of Turbomole. The molecular dynamic runs used a time step of 1.9 fs (80 a.u.) and a Nose-Hoover thermostat[57,58] set to 10 K with a time-constant of 242 fs (10000 a.u.). Initial nuclear velocities were sampled from a

293.15 K Boltzman distribution. Approximate ionisation potentials (IP) for the ground and excited state were, finally, obtained for selected clusters from the differences between the energy of a cation (DFT) and that of the ground state (DFT)/excited state (TD-DFT) at the same geometry, i.e. $IP_{S0} = E_{N+1,DFT} - E_{N,DFT}$ and $IP_{Sn} = E_{N+1,DFT} - E_{N,TD}$ (where E_N is the DFT energy of a system with N electrons). Both the BOMD and IP calculations further use the same approximations (XC-functional, basis-set etc.) as the other DFT and TD-DFT calculations.

Results and discussion

Excited state minima and complexity

As outlined in the introduction previously two general types of minima for nanosized (~ 1 nm) ZnS particles were identified: *N-II* and *I-II* [24], where the *N-II* type minimum was only observed for the S_1 excited state energy surface of the larger particles. For the S_1 excited state energy surface of the smaller nanoparticles and the T_1 excited state energy surface of all the nanoparticles considered only the *I-II* type minimum was observed. The existence of two types of excited state minima for the same particle, differing in localisation of the excited state, raises the question if there are potentially more. For instance, a type *I-I* minimum, previously only observed for Zn_6S_6, and which would be the natural progression in excited state localisation after *N-II* and *I-II*. However, for the larger particles of interest here, direct excited state optimisations for S_1 or T_1 starting from the ground state structure never yield such a minimum (or any other). Therefore, inspiration was taken from the Zn_6S_6 type *I-I* minimum energy structure[22]. Here the distance between the adjacent zinc and sulfur atoms on which the excited state localises becomes dramatically larger (by ~60%) than the same distance in the ground state structure and both atoms become essentially 2-coordinated. One of the Zn-S distances of the type *I-II* minimum structures was thus manually elongated by a similar amount and S_1 and T_1 optimisation were started from this distorted geometry. In the

case of T_1 such optimisations indeed result in a type *I-I* minimum with one zinc and one sulfur atom that are effectively 2-coordinated (see Fig. 3 and section ESI-1 of the supplementary information). Table 1 collates the photoluminescence energy (PLE) and excited state stabilisation energy (ESSE, the difference in excited state energy between the ground state minimum energy geometry and the geometry in question) for the most stable T_1 *I-I* minimum for each particle. A comparison with the values previously found for the T_1 *I-II* minima (see ESI-2) shows that the T_1 *I-I* minima have a lower PLE (~0.3 eV) and are more stable (ESSE ~ 1.25 eV) than their *I-II* counterparts. For S_1, in contrast to the case for T_1, what appears to be a point or more generally a seam where the S_1 and S_0 energy surfaces touch is found (i.e. a CX). The localisation as probed by the difference between ground state and excited state charges at this CX is also approximately *I-I* and the zinc and sulfur atoms on which the excited state localises are effectively 2-coordinated (see Fig. 3). Table 1 also collates the ESSE values for the most stable S_1 *I-I* CX found for each particle (the PLE values are by definition zero). A comparison with the values previously found for the S_1 *N-II* and *I-II* minima (see ESI-2) shows that the S_1 *I-I* CXs are predicted to be more stable (ESSE ~ 1.3 eV) than any of the S_1 minima. It is known that standard TD-DFT by definition cannot correctly describe the specific topology of the energy surfaces in the direct vicinity of a S_1/S_0 CX[59]. This does, however, not stop TD-DFT in practice from relatively accurately predicting both the locations of and the excited state dynamics around CXs when compared to CASSCF (Complete Active Space Self Consistent Field)[60] and/or experimental photochemical[61] results. From a practical point of view the biggest problem is that the CX might be a seam[59,60] (i.e. not a point) and thus less well defined than a simple minima.

Figs. 4 and 5 plot the energy difference of different excited state minima and CXs found for $Zn_{22}S_{22}$ and $Zn_{26}S_{26}$ with respect to the ground state energy for their respective ground state minima. Both figures clearly show that for these lower symmetry particles (compared to e.g.

$Zn_{12}S_{12}$) minima are found to occur in different variants, where the excited state localises on different topologically unique sets of atoms. For instance, as can be seen from Fig. 4, for $Zn_{22}S_{22}$ there are at least two type *N-II* S_1 minima (where the former is 17 meV more stable than the latter) and also two type *I-II* S_1 minima (where the former is 63 meV more stable than the latter) and two *I-II* T_1 minima (where the former is 49 meV more stable than the latter). The fundamental difference between the two sets of minima is the 4-ring involved; either one aligned along the long direction of the particle or one aligned along the radial direction, where localisation on the former yields more stable minima. As can be seen in Fig. 4 one can think of these different sets of minima as different branches or drainage basins with the ground state geometry as watershed. For $Zn_{26}S_{26}$ at this moment only one branch is found but there are likely to exist more and a systematic method of find different excited state minima is desirable. Every type *I-II* minimum of a branch can again give rise to potentially two different type *I-I* minima/CXs depending on which of two sulfur atoms the hole localises. In some cases, these two minima/CXs are degenerate (as for the left branch in Fig. 4) but generally they are not. All these different minima (though not the CXs) can in principle be distinguished directly on basis of their spectroscopic properties. The photoluminescence energy (PLE) of the two *N-II* S_1 minima for $Zn_{22}S_{22}$ for instance differs by 0.05 eV (PLE 2.55 and 2.60 eV), while the PLE of the two *I-II* S_1 minima differs even by 0.12 eV (PLE 0.97 and 0.85 eV). Even relatively simple particles are thus predicted to have a quite complicated excited state energy landscape with many clearly different but typically related minima.

As can be seen from Figs. 4 and 5 (and by comparing the data in table 1 with those in section ESI-2 of the supplementary information) for each particle the PLE decreases and the ESSE increases with increasing localisation (i.e. when going from the *N-II* minimum to the *I-I* minimum/CX). In other words, the more localised a minimum is the more energetically stable it is and the more red-shifted its PLE signal. Also, triplet versions of minima/CXs always are

more stable than singlet versions of the same minima/CXs. Taking this all into account, the fate of an excited state in the larger ZnS nanoparticles is thus predicted to be a localisation or trapping cascade; ground state minimum energy geometry -> type *N-II* minimum -> type *I-II* minimum -> type *I-I* CX. Here the system can relax to the electronic ground state via photoluminescence (fluorescence) at either minimum or radiationless at the CX. The system can also cross from S_1 to T_1 mediated through spin-orbit coupling and the fact that the T_1 type *I-II* minimum lies lower in energy than its S_1 equivalent. In the latter case, the localisation cascade might be; ground state minimum energy geometry (S_1) -> type *N-II* minimum (S_1) -> type *I-II* minimum (S_1) -> type *I-II* minimum (T_1) -> type *I-I* minimum (T_1), followed, perhaps, by a yet undiscovered T_1/S_0 CX. Here the system can additionally relax to the electronic ground state via photoluminescence (phospherence) at either triplet minimum or radiationless at the potential T_1/S_0 CX.

Excited state barriers

Having considered energetics, the next question is kinetics. How large are the barriers between the different minima and what is the chance they will be crossed under typical experimental conditions. As outlined in the methodology section the excited state barrier heights are obtained in a two-step procedure. First the barrier height is approximated through linear interpolation between the structures of the minima. In this way one obtains at least an upper limit to the true barrier height and most likely a reasonable estimate of relative barrier heights at the expense of a limited number of single point calculations along the interpolation path. In a second step, the structure with the highest barrier value along the interpolation path is used as a starting point for a TRIM[56] search for the exact transition state. Fig. 6 shows the energy profile obtained through linear interpolation in the case of $Zn_{22}S_{22}$ (left branch of Fig. 4) while table 2 collates the obtained barrier heights for the singlet minima (focussing on the

barrier between the most stable minima discussed in table 1 and section ESI-2 of the supplementary information).

N-II to I-II barriers

Focussing first on the barrier separating the *N-II* and *I-II* minima. For $Zn_{12}S_{12}$ and $Zn_{16}S_{16}$ there is no *N-II* minimum. However, trajectories for 10 K BOMD runs (inspired by reference 61) for S_1 starting from the ground state minimum energy structure for $Zn_{12}S_{12}$ display a ~300 fs plateau in with roughly the same PLE and ESSE as that observed for the *N-II* minimum in the larger particles (see Figs. S-1 and S-2 in section ESI-3 of the supplementary information). This plateau feature suggests that there might be a proto *N-II* minimum present in these particles and that literally the only thing lacking in these smaller particles is the barrier preventing the excited state to spontaneously collapse into the *I-II* minimum. For $Zn_{22}S_{22}$ and $Zn_{26}S_{26}$ there is a finite barrier between the *N-II* and *I-II* minima but as can be seen from Fig. 6 and table 2 it is predicted to be rather low (approximately 0.15 and 1.15 kT at room temperature). Moreover, the barrier value estimated through interpolation is found to be very similar to that obtained through the full TRIM search. The *N-II* minimum is in most cases thus most likely merely a temporary staging post before the excited state relaxes further to the *I-II* minimum. In this scenario the exact time spent in the *N-II* minimum basin probably depends on the temperature of the particle and the excess energy donated to the particle through interconversion if the initial absorption of light excited the system to S_2 or higher.

On a technical note, it is important to stress that while the calculated *N-II* -> *I-II* barrier values are very low and in the case of $Zn_{22}S_{22}$ barely higher than the inherent energetic uncertainty associated with the use of finite tolerances during a geometry optimisation they are not equal to zero. The found transition states connect two proper minima with only finite positive frequencies (e.g., lowest frequency of the $Zn_{22}S_{22}$ *N-II* minimum is 29 cm^{-1}) and the

optimised transition states themselves have, as required, one imaginary frequency (e.g. in the case of $Zn_{22}S_{22}$ a mode at -69 cm^{-1}).

The fact that in Fig. 6 the barrier, or more strictly the maximum along the interpolation path, for S_1 coincides with a minimum on S_2 suggests that the barrier separating the *N-II* and *I-II* minima might be the result of a strongly avoided crossing between the S_1 and S_2 excited state energy landscapes rather than from the energetic cost of distorting the geometry. Further evidence supporting the strongly avoided crossing hypothesis comes from the analysis of S_1-S_0 and S_2-S_0 charge differences along the interpolation path linking the *N-II* and *I-II* $Zn_{22}S_{22}$ minima. On the *N-II* side of the barrier S_2 has *I-II* like character while on the *I-II* side of the barrier S_2 has *N-II* like character (see Fig. S-3 in section ESI-4 of the supplementary information). In line with what is expected to occur in the case of strongly avoided crossing, the local electronic characters of the S_1 and S_2 energy landscapes exchange. The electronic nature of the barrier might also explain why it is absent for T_1.

I-II to I-I barriers

Calculating the barrier between the *I-II* minima and the *I-I* CX on the S_1 excited state energy landscape is methodologically challenging because, as discussed above, the *I-I* CX is likely to be a seam rather than a point and hence the end point is not necessarily as well-defined as in the case of a minimum. To circumvent this problem, instead a barrier between the *I-II* minimum and the geometry of the *I-I* T_1 minimum was considered as initial guess, exploiting the fact that on the S_1 energy landscape there is a downhill path from the latter well-defined point to the *I-I* CX. In the case of $Zn_{26}S_{26}$ the presence of two different *I-I* T_1 minima for every *I-II* S_1 minimum (see above) results to in two different possible pathways to a *I-I* T_1 minimum and hence two different approximate barriers (0.18 and 0.41 eV respectively), here it was assumed that the lower one is most relevant for actual kinetics and only that structure was used as a starting point for a subsequent TRIM transition state search.

The calculated (approximate) barrier height values in table 2 shows that in the case of the barrier between the *I-II* minima and the *I-I* CX the approximate barrier height value obtained by interpolation is generally much larger (by a factor 10-30) than the true barrier height obtained in the subsequent TRIM transition state search. Just as for their *N-II* to *I-II* counterparts the obtained transition states had one negative frequency (e.g. in the case of $Zn_{12}S_{12}$ a mode at -32 cm^{-1} and one at -49 cm^{-1} for $Zn_{22}S_{22}$). Moreover, excited state optimisation runs started from initial structures obtained by slightly distorting the transition state structure along the imaginary mode find in one direction the *I-II* minimum and in the other direction the *I-I* CX, further confirming that the transition states obtained in the TRIM searches are proper transition states. Figure 7 displays the obtained *I-II* -> *I-I* transition state geometry for $Zn_{12}S_{12}$.

Concentrating on the TRIM values, table 2 shows that the *I-II* minima and the *I-I* CX barriers are predicted to be of the same order of magnitude as their *N-II* to *I-II* counterparts (0.2-1.4 kT at room temperature). The *I-II* minima are under experimental conditions thus most likely also mere temporary staging posts on the inevitable path to the *I-I* CX. The time spent by the system in the *I-II* minima and the odds of observing its characteristic fluorescence is thus predicted to depend, just as in the case of the *N-II* minima, critically on the exact experimental conditions employed. With only low barrier separating the different excited state minima and the CX it is likely that radiationless de-excitation will be competitive with fluorescence, something we hope to further explore using BOMD and the surface-hopping approach to non-adiabatic abintio MD[60,61,62,63] approach to excited state nuclear dynamics in the future (see also perspective section below).

De-excitation and alternative ground state structures

Finally, the energy profile in Fig. 6 also shows a small barrier on the ground state energy surface between the geometries of the *I-II* minimum and *I-I* CX. Such a barrier on the ground

state surface could mean that after relaxing back to the ground state at the T_1 *I-I* minimum (phospherence) or at the S_1 *I-I* CX (radiationless) the system might not be able to relax back to the original ground state minimum the system was excited from. Indeed in the case of $Zn_{22}S_{22}$ a ground state DFT optimisation starting from these points results in a different ground state minimum where one of the sulfur atoms is inverted and puckered inwards and that lies 0.22 eV higher in energy (see Fig. S-4 in section ESI-5 of the supplementary information for a comparison between both ground state structures). In this particular case, the two minima are topologically the same and there is likely only a relatively moderate barrier on the ground state energy landscape for converting the structure back into the starting $Zn_{22}S_{22}$ global minimum structure (interpolation between both minima yields an estimate of the barrier height of 0.28 eV, see Fig. S-5 in section ESI-5 of the supplementary information for a comparison between both ground state structures). However, in other cases the system might relax into a topologically different ground state minimum separated from the global minimum by a larger barrier that is unlikely to be crossed and the net result after de-excitation is a defected structure.

Perspective

The above analysis focussed on series of ~ 1 nm ZnS nanoparticles but there is no inherent reason why such cascades of excited state minima could not exist for other types of inorganic nanoparticles or perhaps even be a common feature for inorganic nanoparticles in general. Larger nanoparticles or nanoparticles of different materials might be more rigid with more atoms having the coordination number found for the bulk material but surface atoms will always be relatively free to move. In particular, the existence of a barrier that hinders full excited state localisation (i.e. the formation of an *I-I* minimum where an excited electron and hole are each trapped on one atom) and thus the existence of at least a minimum where an excited electron and/or hole are trapped by a unit involving more than one atom (e.g. the *I-II*

minimum here) might be a relatively common feature on the excited state energy landscape of other inorganic nanoparticles.

Clearly for these ZnS nanoparticles the cartoon model of excited state relaxation in inorganic nanoparticles that involves relaxation to the bottom of only one approximately harmonic well from where then the PL takes places is too simplistic. Future experimental and theoretical work should carefully consider the role of temperature, excess energy and the time scale of the experiment (e.g. the time delay between, for instance, absorption and PL). From a computational point of view this raises a difficult question; how to systematically find the relevant excited state minima beyond those directly connected to the ground state minima structure by an energetic down hill path and the barriers between them. The procedure employed in this paper is to an extent *ad hoc* while BOMD and the surface-hopping approach to non-adiabatic *ab-intio* MD, which explicitly considers hopping between different (excited state) energy surfaces during the *ab-initio* MD, is for the moment only numerically tractable for just the smallest particles (also as a number of independent runs will be required). Moreover, careful thought is required when using MD about how to properly include the dissipation of heat to the environment. The usage of methods developed for the systematic exploration of ground state energy surfaces (e.g. basin-hopping[64] and genetic algorithm[65,66] based global optimisation) might present an alternative way forward. However, for the moment such methods are probably also only numerically tractable for merely the smallest systems, as they typically require a very large number of independent energy/gradient evaluations (e.g. 10.000+).

From an application point of view an important side effect of the localisation cascade is the change in the ability of the excited electrons or formed holes to drive chemical reactions or an external electric circuit. The key parameters in the TD-DFT total energy picture (in contrast to the traditional orbital picture) are he relative energies of an electron in the ground and

excited state relative to that of the vacuum level, i.e. the negative of the ground state and excited state ionisation potentials. As can be seen from table 3 the predicted ground and excited state ionisation potentials change drastically when going from the ground state minimum energy geometry down the localisation cascade, where the ground state ionisation potential becomes less positive (and the relative energy of an electron in the ground state thus less negative) while the excited state ionisation potential becomes more positive (and the relative energy of an electron in the first excited state thus more negative). This suggests that down the localisation cascade the ability of an excited nanoparticle to drive reactions, such as the half reactions of the water splitting reaction, or an external electric circuit changes. The ground and excited state ionisation potentials at the ground state geometries (or their HOMO/LUMO counterparts) thus only tell a part of the story when it comes to a material being suitable as, for example, a photocatalyst. Again relative timescales, in this case those of electron/hole transfer versus that of the nuclear relaxation responsible for the localisation or trapping cascade, are a key parameter in understanding both experiment and theory.

Conclusions

In conclusion, the fate of excited states for ZnS nanoparticles is predicted to involve a cascade of excited state minima, separated by excited state barriers, and ending up in a conical intersection between the excited state energy surface and the ground state. The different minima found differ in the localisation of the excited state, where minima further down the cascade display more localised excited states. The excited state barriers between the different minima and the conical intersection are predicted to be rather low (0.2-1.5 kT) and hence radiationless de-excitation via the conical intersection is likely to be competitive with fluorescence. There is no inherent reason why a similar localisation or trapping cascade could not also occur for larger nanoparticles or inorganic nanoparticles of other materials than zinc sulfide.

Acknowledgements

I kindly acknowledge Mr. Enrico Berardo, Prof. S.T. Bromley, Prof. F. Furche, Prof. A. Shluger, Dr. A.A. Sokol and Dr. S.M. Woodley for stimulating discussion and the UK Engineering and Physical Sciences Research Council (EPSRC) for a Career Acceleration Fellowship (Grant EP/I004424/1). Computational time on the computers of the Legion High Performance Computing Facility at University College London, the IRIDIS regional high-performance computing service provided by the e-Infrastructure South Centre for Innovation (EPSRC Grants EP/K000144/1 and EP/K000136/1) and on HECToR the UK's national high-performance computing service (via our membership of the UK's HPC Materials Chemistry Consortium, which is funded through EPSRC grant EP/F067496) is gratefully acknowledged.

References

[1] A. Fujishima, K. Hondo, Nature, 1972, **238**, 37.

[2] K. Maeda, J. Photochem. Photobio C: Photochem. Rev., 2011, **12**, 237.

[3] F.E. Osterloh, Chem. Soc. Rev, 2013, DOI 10.1039/c2c35266d

[4] B. O'Regan, M. Grätzel, Nature, 1991, **353**, 737.

[5] X. Chen , C. Li , M. Grätzel , R. Kostecki, S.S. Mao, Chem. Soc. Rev., 2012,**41**, 7909.

[6] A. Hagfeldt, G. Boschloo, L. Sun, L. Kloo, H. Pettersson, Chem. Rev. 2010, **110**, 6595

[7] M. Bruchez, M. Moronne, P. Gin, S. Weiss and A.P. Alivisatos, Science 1998, **281**, 2013.

[8] K.H. Lee, J. Nucl. Med. 2007, **48**, 1408.

[9] T.J. Deerinck, Tox. Path. 2008, **36**, 112.

[10] M. Kasha, Discuss. Faraday Soc., 1950, **9** 14.

[11] M. Beer, H. C. Longuet-Higgins, J. Chem. Phys., 1955, **23,** 1390.

[12] C.L. Choi, H. Li, A.C.K. Olson, P.K. Jain, S. Sivasankar, A.P. Alivasatos, Nano Letters, 2011, 11, 2358.

[13] E. Runge, and E. K. U. Gross, Phys. Rev. Lett. 1984, **52**, 997.

[14] F. Furche and R. Ahlrichs, J. Chem. Phys. 2002, **117**, 7433.

[15] F. Furche and R. Ahlrichs, J. Chem. Phys. 2004, **121**, 12722.

[16] D. Rappoport and F. Furche in Time Dependent Density Functional Theory, Lect. Notes Phys. 706 (Springer, Berlin, 2006).

[17] D. Sundholm, Phys. Chem. Chem. Phys. 2004, **6**, 2044.

[18] X. Wang, R. Q. Zhang, S. T. Lee, T. A. Niehaus and Th. Frauenheim, Appl. Phys. Lett. 2007, **90**, 123116.

[19] Y. Wang, R. Zhang, T. Frauenheim and T.A. Niehaus, J. Phys. Chem. C 2009, **113**, 12935.

[20] M.A. Zwijnenburg, A.A. Sokol, C. Sousa and S.T. Bromley, J. Chem. Phys. 2009, **131**, 034705.

[21] V. E. Matulis, D. M. Palagin and O. A. Ivashkevich, Rus. J. Gen. Chem. 2010, **80**, 1078.

[22] M.A. Zwijnenburg, C. Sousa, F. Illas, S.T. Bromley J. Chem. Phys. 2010, **134**, 064511.

[23] M.A. Zwijnenburg, F. Illas, S.T. Bromley, Phys. Chem. Chem. Phys. 2011, **13,** 9311.

[24] M.A. Zwijnenburg, Nanoscale 2012, **4**, 3711.

[25] W.G. Becker and A.J. Bard, J. Phys. Chem. 1983, **87**, 4888.

[26] A.A. Khosravi, M. Kundu, L. Jatwa, S.K. Deshpande, U.A. Bhagwat, M. Sastry and S.K. Kulkami, Appl. Phys. Lett. 1995, **67**, 2702.

[27] W. Chen, Z.G. Wang, Z.J. Lin and L.Y. Lin, J. Appl. Phys. 1997, **82**, 3111.

[28] W. Chen, Z. Wang, Z. Lin and L. Lin, Appl. Phys. Lett. 1997, **70**, 1465.

[29] N. Arul Dhas, A. Zaban and A. Gedanken, Chem. Mater. 1999, **11**, 806.

[30] W.S. Chae, J.H. Yoon, H. Yu, D.J. Jang and Y.R. Kim, J. Phys. Chem. B 2004, **108**, 11509.

[31] D.J. Jovanovic, I.L. Validzic, I.A. Jankovic, N. Bibic and J.M. Nedeljkovic, Mat Let. 2007, **61**, 4396.

[32] J.S. Hu, L.L. Ren, Y.G. Guo, H.P. Liang, A.M. Cao, L.J. Wan, C.L. Bai, Angew. Chem. Int. Ed., 2005, **117**, 1295.

[33] D. Chen, F. Huang, G. Ren, D. Li, M. Zheng, Y. Wang, Z. Lin, Nanoscale, 2011, 2, 2062.

[34] M.A. Zwijnenburg, Nanoscale 2011, **3**, 3780.

[35] J.M. Matxain, A. Irigoras, J.E. Fowler and J.M. Ugalde, Phys. Rev. A, 2000, **63,** 013202.

[36] J.M. Matxain, A. Irigoras, J.E. Fowler and J.M. Ugalde, Phys. Rev. A, 2001, **64**, 013201.

[37] J.M. Matxain, L.A. Eriksson, J.M. Mercero, J.M. Ugalde, E. Spano, S. Hamad and C.R.A. Catlow, Nanotechnology, 2006, **17**, 4100.

[38] J. Azpiroz, E. Mosconi and F. De Angelis, J. Phys. Chem. C. 2011, **115**, 25219.

[39] G. Malloci , L. Chiodo, A. Rubio, and A. Mattoni, J. Phys. Chem. C. 2012, **116**, 8741.

[40] C. Caddeo, G. Malloci , L. Chiodo, F. De Angelis, L. Colombo and A. Mattoni, Phys. Chem. Chem. Phys.. 2012, **14**, 14293.

[41] E. Spano, S. Hamad and C.R.A. Catlow, J. Phys. Chem. B, 2003, **107**, 10337.

[42] E. Spano, S. Hamad and C.R.A. Catlow, Chem. Commun., 2004, 864.

[43] S. Woodley, A. Sokol and C.R.A. Catlow, Z. Anorg. Allg. Chem., 2004, **630**, 2343.

[44] S. Hamad, C.R.A. Catlow and E. Spano, J. Phys. Chem. B, 2005, **109**, 2703.

[45] A. Burnin, E. Sanville and J.J. BelBruno, J. Phys. Chem. A, 2005, **109**, 5026.

[46] S. Hamad and C.R.A. Catlow, J. Cryst. Growth, 2006, **294**, 2.

[47] R. Ahlrichs, M. Baer, M. Haeser, H. Horn, and C. Koelmel, Chem. Phys. Lett., 1989, **162**, 165.

[48] O. Treutler and R. Ahlrichs, J. Chem. Phys., 1995, **102**, 346.

[49] M. v. Arnim and R. Ahlrichs, J. Comp. Chem., 1998, **19**, 1746.

[50] Von Wuellen, C., J. Comput. Chem. 2011, **32**, 1995.

[51] A.D. Becke, J. Chem. Phys. 1993, **98**, 5648.

[52] A. Schafer, H. Horn, R. Ahlrichs, J. Chem. Phys., 1992, **97**, 2571.

[53] S. Hirata and M. Head-Gordon, Chem. Phys. Lett, 1999, **314**, 291.

[54] M.J.G. Peach, M.J. Williamson and D.J. Tozer, J. Chem. Theory Comput., 2011, **7**, 3578.

[55] F. Plasser, http://homepage.univie.ac.at/felix.plasser/struc_manip/struc_manip_doc.htm.

[56] T. Helgaker, Chem. Phys. Lett., 1991, **182**, 503.

[57] S. Nose, J. Chem. Phys., 1984, **81**, 511.

[58] W.G. Hoover, Phys. Rev. A, 1985, **31**, 1695.

[59] B.G. Levine, C. Ko, J. Quenneville, T.J. Martinez, Mol. Phys., 2006, **104**, 1039.

[60] E. Tapavicza, I. Tavernelli, U. Rothlisberger, C. Filippi, M.E. Casida, J. Chem. Phys., 2008, **129**, 124108.

[61] E. Tapavicza, A.M. Meyer and F. Furche, Phys. Chem. Chem. Phys. 2011, **13**, 20986.

[62] J. C. Tully, J. Chem. Phys. 1990, **93,** 1061.

[63] E. Tapavicza, I. Tavernelli, and U. Rothlisberger, Phys. Rev. Lett. 2007, **98,** 023001.

[64] D. J. Wales and J.P.K. Doye, J. Phys. Chem. A, 1997, **101**, 5111.

[65] R.L. Johnston, Dalton Trans., 2003, 4193.

[66] S.M. Woodley, A.A. Sokol and C.R.A. Catlow, Z. Anorg. Chem., 2004, **630**, 2343.

Table 1 PLE and ESSE for the most stable *I-I* type T_1 minima and S_1 CX found for the studied nanoparticles (all energies in eV, CX values given to only one decimal because of the inherent difficulty in defining the precise location of the CX highlighted in the text). ESSE-S values give the position of the T_1 minima relative to the energy of the S_1 state at the ground state minimum energy geometry.

Table 2 Barrier height values calculated for the transition states between the different S1 minima/CX types found for the studied nanoparticles (all barrier heights in eV, approximate values obtained through interpolation given in parentheses, barriers height values smaller than 0.01 eV not explicitly given).

Table 3 IP_{S0} and IP_{S1} values calculated for the different S_1 minima and CX found for the $Zn_{22}S_{22}$ nanoparticle (all values in eV).

Figure 1 Cartoon representation of a ground and excited state energy landscape highlighting some of the processes discussed in the text.

Figure 2 DFT optimised ground state structures for the global minima candidates used in this study: (I) $Zn_{12}S_{12}$, (II) $Zn_{16}S_{16}$, (III) $Zn_{22}S_{22}$ and (IV) $Zn_{26}S_{26}$.

Figure 3 Atomic geometries around the atoms on which the excited state localises for the *I-I* T_1 minimum and *I-I* S_1 CX found for the $Zn_{12}S_{12}$ nanoparticle (all distances in Angstrom, for comparison ground state Zn–S distance in a 4-membered ring is 2.35 Å and outside 2.27 Å).

Figure 4 Plot of the energy difference of different excited state minima and CXs found for $Zn_{22}S_{22}$ with respect to the ground state energy at the ground state minima (PLE values given in labels, singlet states black diamonds, triplet states open squares, arrows and circles highlight the 4-ring involved with either branch).

Figure 5 Plot of the energy difference of different excited state minima and CXs found for $Zn_{26}S_{26}$ with respect to the ground state energy at the ground state minima (PLE values given

in labels, singlet states black diamonds, triplet states open squares, arrow highlights the 4-ring involved). The second *I-I* S_1 CX is predicted to lie slightly higher than expected from the trend in the T_1 minima, which might be real, or alternatively, the result of the problems highlighted in the text with finding the exact location of a CX.

Figure 6 Energy profile along the interpolated path that connects the ground state minimum energy geometry with those of the different S_1 excited state minima found for $Zn_{22}S_{22}$.

Figure 7 Transition state structure found for the barrier separating the *I-II* minimum and the *I-I* CX for $Zn_{12}S_{12}$ (structural changes larger than 1% highlighted, all distances in Angstrom, for comparison the relevant Zn–S distance in the *I-II* minimum is 2.66 Å).

	T_1 *I-I*			S_1 *I-I*
	PLE	ESSE	ESSE-S	ESSE
$Zn_{12}S_{12}$	0.31	1.29	1.37	1.3
$Zn_{16}S_{16}$	0.27	1.25	1.32	1.3
$Zn_{22}S_{22}$	0.29	1.23	1.30	1.2
$Zn_{26}S_{26}$	0.28	1.24	1.31	1.2

S_1	*N-II -> I-II*	*I-II -> I-I*
	Barrier	Barrier
$Zn_{12}S_{12}$	--	< 0.01 (0.08)
$Zn_{16}S_{16}$	--	0.02 (0.18)
$Zn_{22}S_{22}$	< 0.01 (< 0.01)	0.04 (0.24)
$Zn_{26}S_{26}$	0.02 (0.03)	< 0.01(0.18)

	Ground state	*N-II*	*I-II*	*I-I*
IP_{S1}	4.3	4.7	6.2	6.8
IP_{S0}	8.1	7.3	7.0	6.8

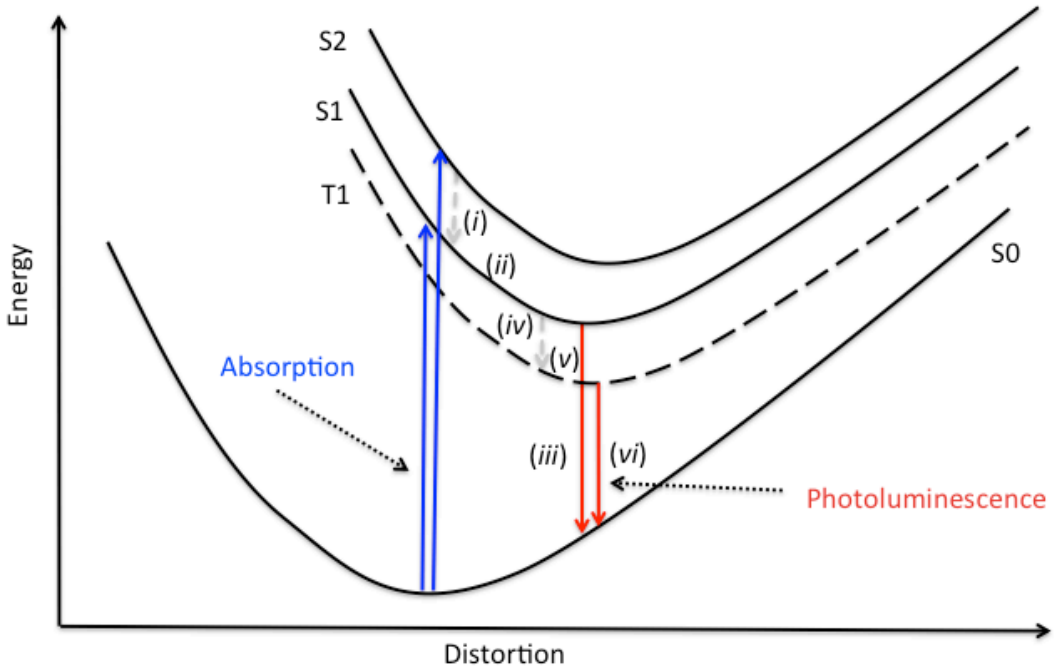
S2
S1
T1
S0
(i)
(ii)
(iii)
(iv)
(v)
(vi)
Absorption
Photoluminescence
Energy
Distortion

I

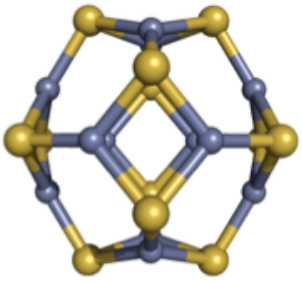

III

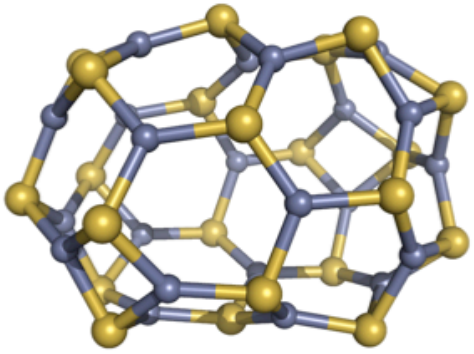

II

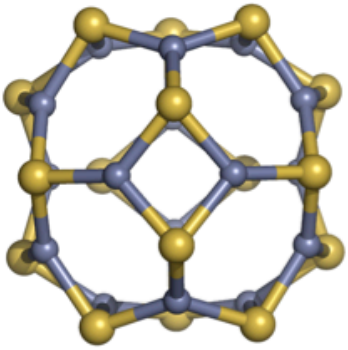

IV

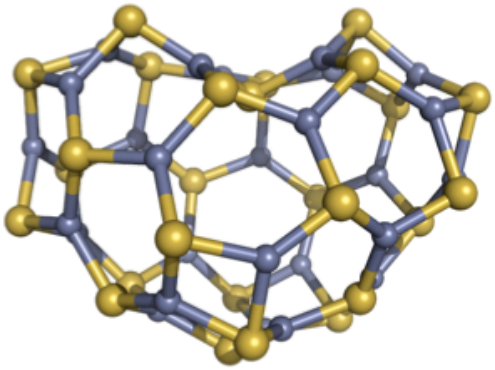

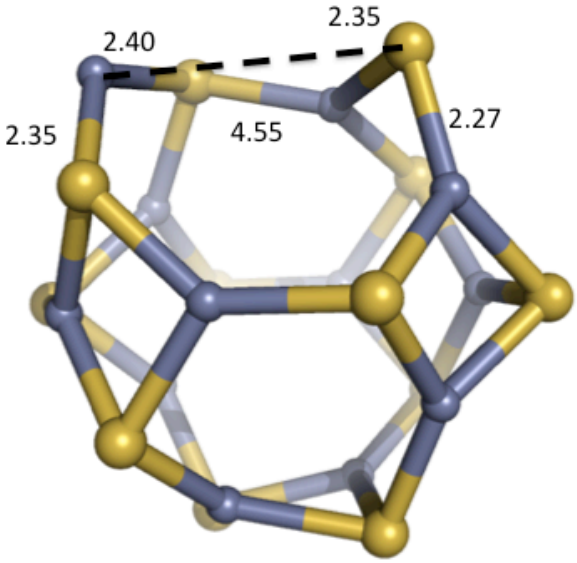

I-I T_1 min

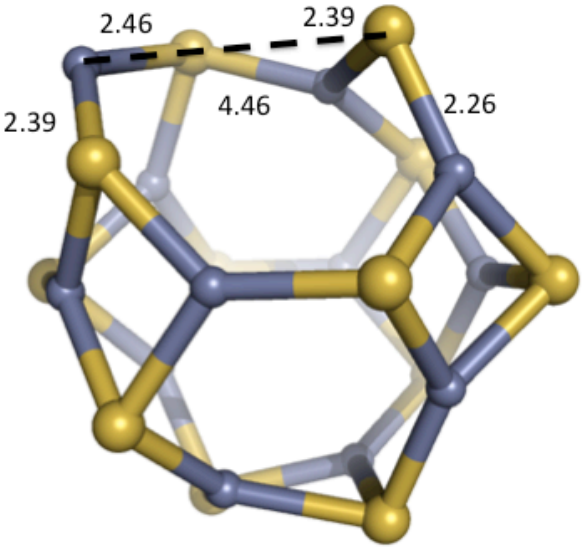

I-I S_1 CX

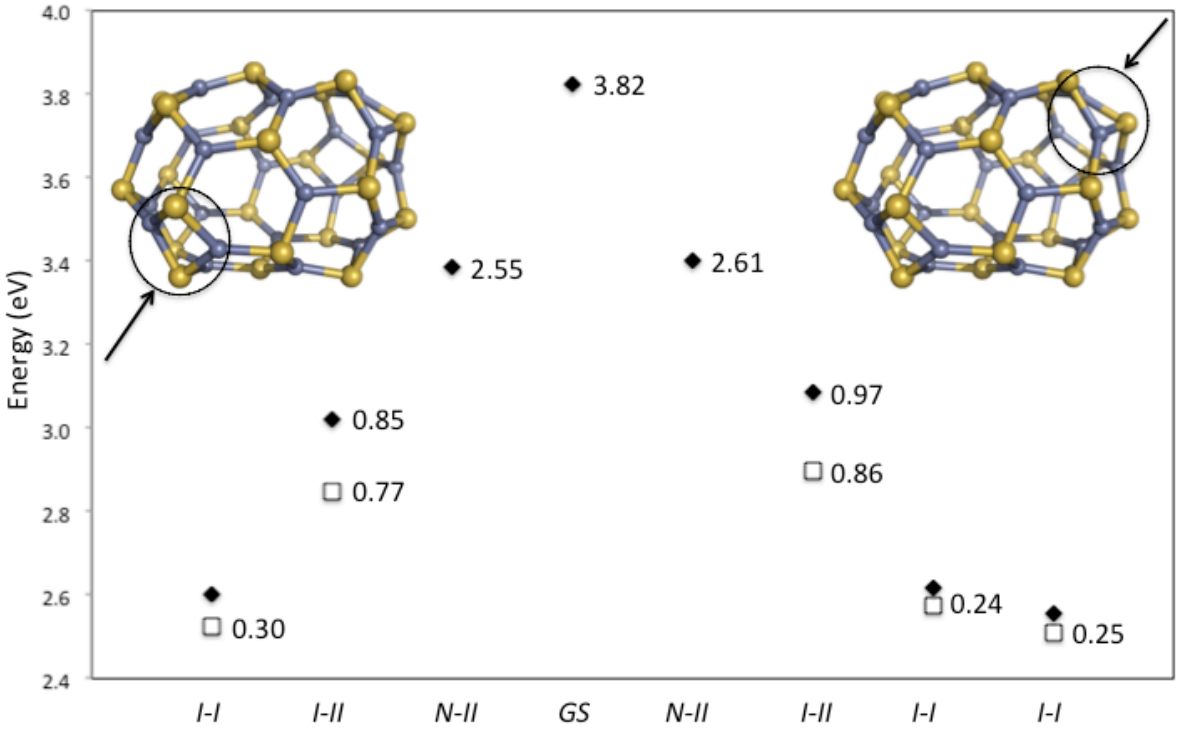
Energy (eV)
4.0
3.8
3.6
3.4
3.2
3.0
2.8
2.6
2.4
3.82
2.55
2.61
0.97
0.85
0.86
0.77
0.30
0.24
0.25
I-I
I-II
N-II
GS
N-II
I-II
I-I
I-I

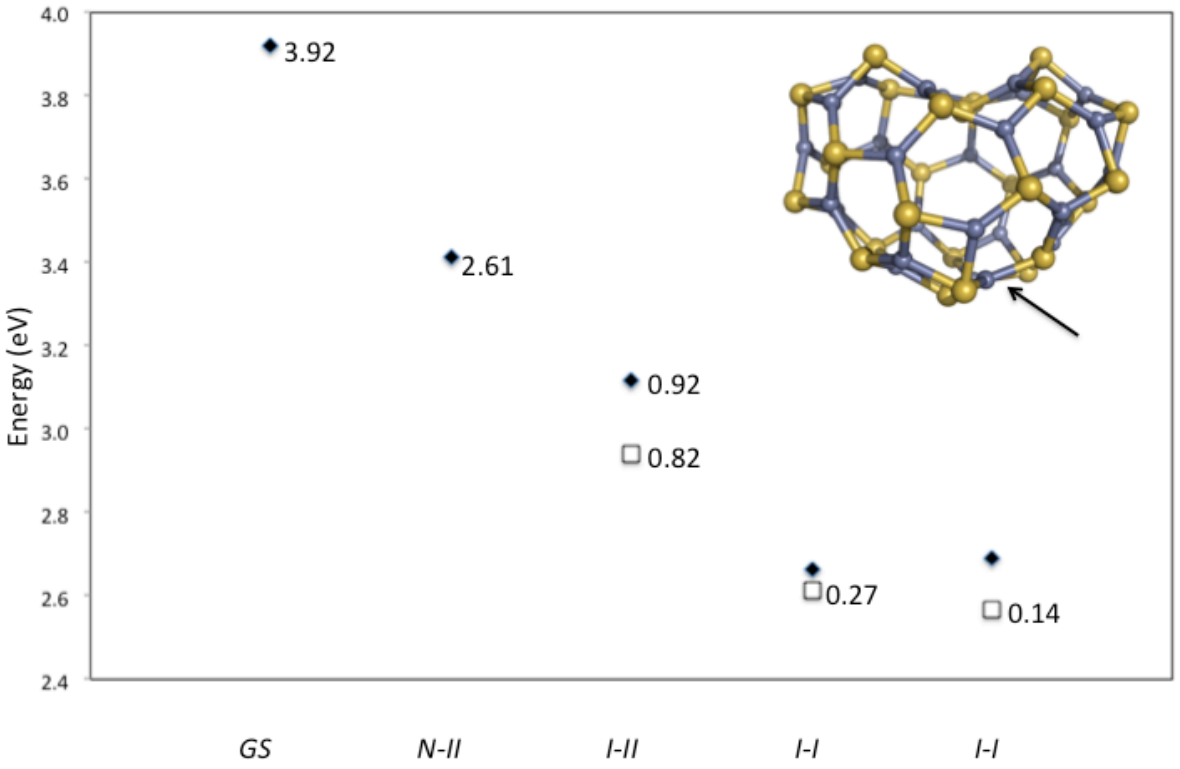
Energy (eV)
4.0
3.8
3.6
3.4
3.2
3.0
2.8
2.6
2.4
3.92
2.61
0.92
0.82
0.27
0.14
GS
N-II
I-II
I-I
I-I

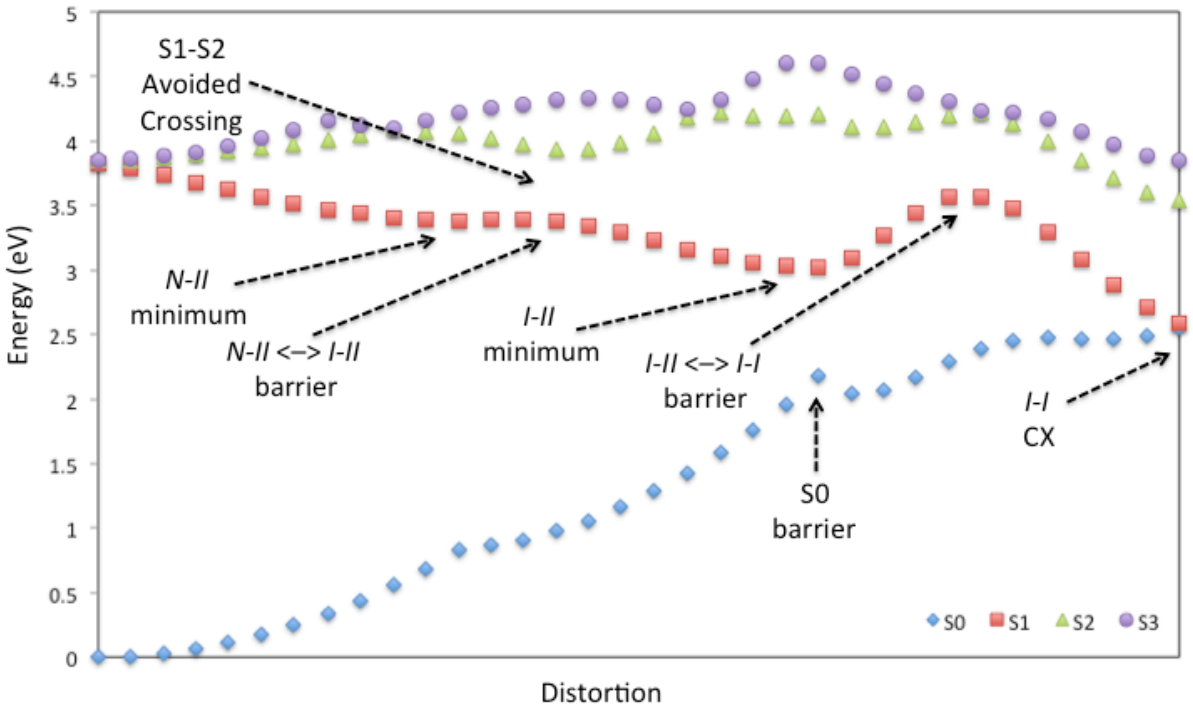
S1-S2
Avoided
Crossing
N-II
minimum
N-II <–> I-II
barrier
I-II
minimum
I-II <–> I-I
barrier
S0
barrier
I-I
CX
S0
S1
S2
S3
Energy (eV)
Distortion
0
0.5
1
1.5
2
2.5
3
3.5
4
4.5
5

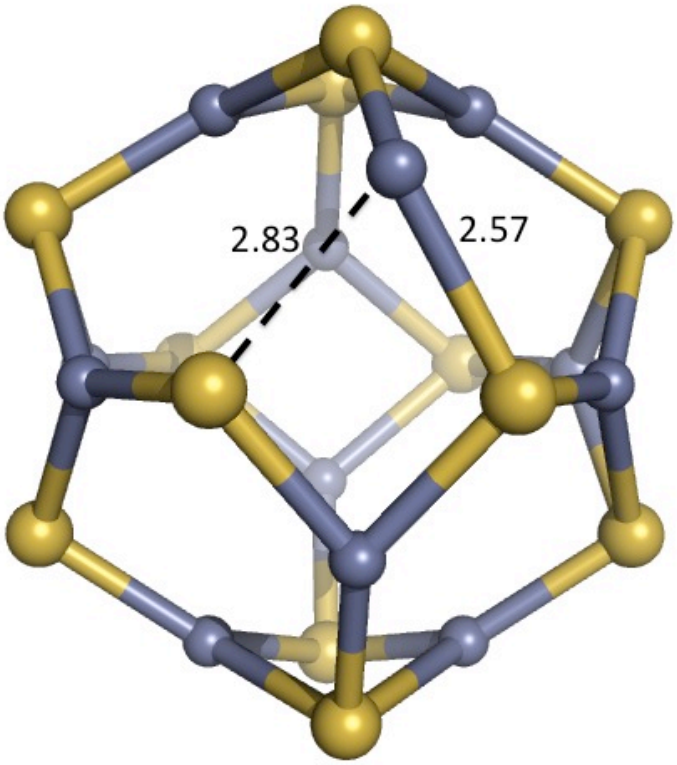
2.83
2.57